

Ultra-Sensitive and Selective Electrochemical Bio-Fluid Biopsy for Oral Cancer Screening

Zuohui Xiao, Chenyan Huang, Shengjie Jiang, Xiangyu Kong, Yunfei Teng, Bo Niu, Congcong Zhu, Weiwen Xin, Xiaohui Chen, Liping Wen, Yan Wei,* and Xuliang Deng

The early diagnosis of recurrence and metastasis is critically important for decreasing the morbidity and mortality associated with oral cancers. Although liquid biopsy methods hold great promise that provide a successive “time-slice” profile of primary and metastatic oral cancer, the development of non-invasive, rapid, simple, and cost-effective liquid biopsy techniques remains challenging. In this study, an ultrasensitive and selective electrochemical liquid biopsy is developed for oral cancer screening based on tracking trace amounts of cancer biomarker by functionalized asymmetric nano-channels. Detection via antigen–antibody reactions is assayed by evaluating changes in ionic current. Upon the recognition of cancer biomarker antigens in bio-fluids, the inner wall of nano-channel immobilized with the corresponding antibodies undergoes molecular conformation transformation and surface physicochemical changes, which significantly regulate the ion transport through the nano-channel and help achieve sensitivity with a detection limit of 10^{-12} g mL⁻¹. Furthermore, owing to the specificity of the monoclonal antibody for the antigen, the nano-channel exhibits high selectivity for the biomarker than for structurally similar biological molecules present in bio-fluids. The effectiveness of this technique is confirmed through the diagnosis of clinical cases of oral squamous cell carcinoma. This study presents a novel diagnostic tool for oral cancer detection in bio-fluids.

approximately 500 000 new cases and 150 000 deaths recorded annually, imposes a significant burden on the global economy.^[1] This can be attributed to the delayed detection of local tumor recurrence and peripheral metastasis, which significantly compromises the effectiveness of clinical therapy and decreases the survival rate of oral cancer.^[2] Therefore, methods that facilitate the early diagnosis of recurrence and metastasis are urgently required to decrease the morbidity and mortality arising from complications in oral cancers.

Tissue biopsy is the gold standard for oral cancer diagnosis, which is used by clinicians for the direct detection of subtle structural abnormalities and evaluation of tumor aggressiveness.^[3] However, since the method is invasive, expensive, and laboratory-based, its repeated application during long observation periods can be challenging.^[4] Moreover, disease development commences significantly earlier than the appearance of lesions.^[5] Therefore, increasing efforts have been made to address the development of practicable

1. Introduction

Oral cancer is a global medical threat that deeply affects various sections of the society. The high mortality of oral cancer, with

and non-invasive early assessment methodologies. In this sense, bio-liquid biopsy for the detection of oral cancer biomarkers has emerged as a revolutionary alteration to traditional detection methods.^[6] Bio-liquid biopsy and imaging-guided cancer therapy are now rapidly emerging as powerful precision cancer theranostic paradigm, as they can offer both diagnostic information and therapeutic benefits.^[7] As a non-invasive diagnostic tool, bio-liquid biopsy can help obtain a successive “time-slice” profile of primary and metastatic oral cancer rather than snapshots at selected time points.^[8] Thus, it is an efficient method for the detection of early evidences of oral cancer occurrence or re-emergence that can help clinicians in therapeutic decision-making.^[9] To date, several methods have been introduced for liquid biopsy in cancer, including enzyme-linked immunosorbent assay (ELISA),^[10] enzyme-amplified lanthanide luminescence,^[11] radioimmunoassay,^[12] immuno-polymerase chain reaction assay,^[13] matrix-assisted laser desorption,^[14] and selected reaction monitoring mass spectrometry.^[15] However, commercially available sensors are either susceptible to inhibition caused by alterations in enzymatic activity or reaction conditions, or require highly qualified personnel and sophisticated instrumentation for operation. Conversely, other emerging techniques, including arrays based on optical, electrochemical, and nano-transistor

Dr. Z. Xiao, Dr. C. Huang, Dr. S. Jiang, Prof. Y. Wei, Prof. X. Deng
Beijing Laboratory of Biomedical Materials
Department of Geriatric Dentistry
Peking University School and Hospital of Stomatology
Beijing 100081, P. R. China
E-mail: kqweiyang@bjmu.edu.cn

Prof. X. Kong, Prof. L. Wen, Dr. Y. Teng, Dr. B. Niu, Dr. C. Zhu, Dr. W. Xin
CAS Key Laboratory of Bio-inspired Smart Interfacial Science Technical
Institute of Physics and Chemistry
Chinese Academy of Sciences
29 Zhongguancun East Road, Haidian District, Beijing 100190, P. R. China
Dr. X. Chen
Division of Dentistry
School of Medical Sciences
The University of Manchester
Oxford Road, Manchester M13 9PL, UK

 The ORCID identification number(s) for the author(s) of this article can be found under <https://doi.org/10.1002/smt.202001205>.

DOI: 10.1002/smt.202001205

detection, are mostly in developmental stages and are yet to be used for diagnosing clinical cases.^[16] Therefore, the development of a non-invasive, rapid, simple, cost-effective, and clinically applicable liquid biopsy technique with high performance efficiency is critical for prognosis prediction as well as for directing clinical therapeutic strategies.

Oral squamous cell carcinoma (OSCC) accounts for 95% of oral cancers and is ranked the sixth leading cause of cancer-related deaths worldwide.^[17] Although a panel of tumor markers including circulating proteins, tumor cells, tumor DNA and exosomes have been unveiled to be indicative for the presence of OSCC, Cystatin B (CSTB) was recently demonstrated to be a sensitive and independent predictor for the local recurrence of OSCC that can help distinguish between patients with and without lymph node metastasis.^[18] As such, by monitoring subtle changes in CSTB levels in body fluids, clinicians may obtain a promising and reliable pre-clinical diagnosis of the primary tumor; regional lymph nodes; distant metastasis classification of OSCC for designing therapeutic strategies.

Herein, we developed an ultra-sensitive and selective electrochemical liquid biopsy method for oral cancer screening that could be used to track trace levels of CSTB using functionalized asymmetric nano-channels. The detection was assayed based on changes in ionic current induced by the antigen–antibody immunoreaction between CSTB in bio-fluid samples and antibodies immobilized on the nano-channel. Besides ultra-sensitivity, owing to the binding ability of the monoclonal antibody to the antigen, the nano-channels also exhibited high selectivity for CSTB than for coexisting structurally similar biological molecules present in the bio-fluid samples. The effectiveness of this technique was also confirmed in clinical cases of OSCC.

2. Results and Discussion

2.1. Fabrication of the Functionalized Nano-Channel System

We used CSTB as a biomarker model to develop the novel liquid biopsy technique for oral cancer screening. As shown

in the schematic in **Figure 1** the conical nano-channel was functionalized by the immobilization of CSTB-specific monoclonal antibodies on the inner wall. Next, CSTB detection was specifically observed to induce variations in the microenvironment of the modified nano-channel, which triggered sensitive changes in the transmembrane current. The entire detection process was performed by monitoring the transformation in the ionic current in the nano-channel and analyzing the rectification ratio of the current. In this study, polyethylene terephthalate (PET) of 12- μm thickness was irradiated with swift heavy ions (Au) to form the single-channel track.^[19] The nano-channel was fabricated by asymmetric etching along the track, and the single structure improved the detection sensitivity.^[20] As such, after the hydrolysis of the alkaline etching solution along the channel track, the conical nano-channel (**Figure 2A**) with a large opening diameter of ≈ 500 nm (base side, **Figure 2B**) and a small opening diameter of ≈ 10 nm (tip side, **Figure 2C**) was developed and visualized using a scanning electron microscopy. This structure was similar to that of nano-molecular detection devices with a high rectification effect reported in an earlier studies.^[21] Therefore, the precise morphology of the nano-channel could help detect minor molecular differences based on changes in the ionic current and rectification ratio. After etching, a large number of carboxyl groups ($-\text{COOH}$) were exposed on the inner wall of the PET nano-channel after polymeric chain hydrolysis, which were subsequently activated by treating with 1-ethyl-3-(3-dimethylaminopropyl) carbodiimide/*N*-hydroxysulfosuccinimide sodium salt. The CSTB-specific monoclonal antibody equipped with an amino group ($-\text{NH}_2$) was added to facilitate the specific immunoreaction that would modify the nano-channel to realize functionalization. Furthermore, as shown in **Figure 2D**, observation of the specimen using transmission electron microscopy (TEM) showed that the diameters of the antibodies and CSTB were both less than 5 nm, which was significantly lesser than the diameter of the nano-channel. This ensured that adequate space was available for antibody modification and CSTB detection. Based on conformation obtained via TEM, the diameter combination complex

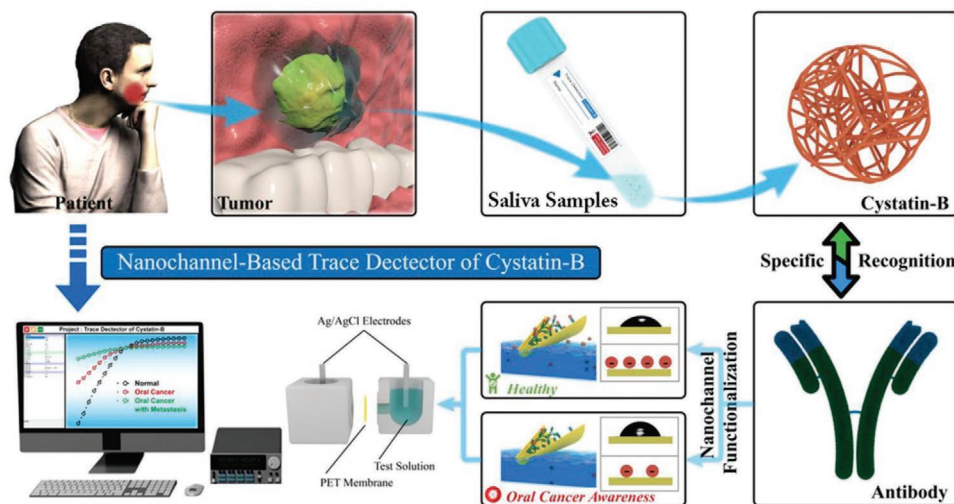


Figure 1. Designing functionalized asymmetric nano-channels for ultra-sensitive and selective cancer screening based on tracking of trace levels of cancer biomarkers. Saliva samples were collected from patients and tested using the nano-channel system. Based on the surface electricity and wettability transformation, a sensitive and selective assay could be accomplished for trace level biomarker detection.

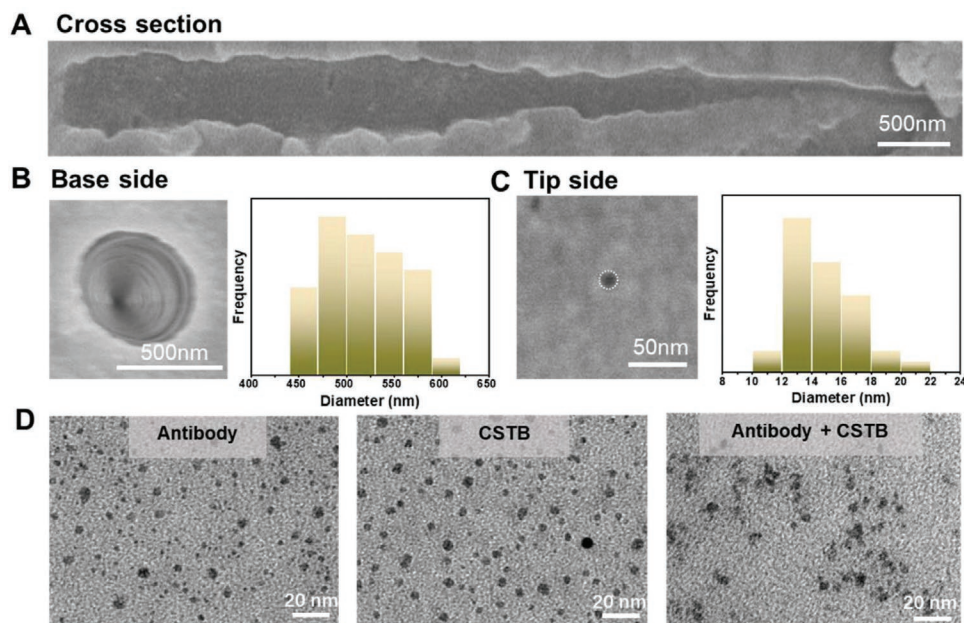


Figure 2. SEM images of biological nano-channels. A) The conical nano-channel was first observed using a vertical section of the membrane. B,C) Typical images and statistical data for the base side and the tip side of nano-channels are presented. Conical nano-channels with opening diameter of approximately 500 nm and ending diameter of approximately 50 nm; D) TEM images depicting the basic morphologies of anti-CSTB antibody, CSTB (antigen), and their immunoreaction complex. The dimensions were appropriate for the nano-channel. CSTB, cystatin B; SEM, scanning electron microscopy; TEM, transmission electron microscopy.

increased marginally after the immunoreaction occurred in the solution (right panel of Figure 2D), which laid the foundation for the spatial structure transformation in the inner wall of the nano-channel.

2.2. Characterization of the Functionalized Nano-Channel System

A stable connection between the antibodies and the nano-channel membrane was essential for local reaction and accurate detection. To enable this, we modified the planar PET membrane using a multi-nano-channel of the same material. After the equal etching and activation processes, the membrane was rinsed several times to complete a series of characterization tests. First, the section of the membrane connected to the modified antibody showed a second antibody fluorescence area when observed under a laser confocal microscope (Figure 3A, top), whereas the control group (Figure 3A, bottom) showed almost no specific fluorescence. The images indicate the location and morphology of the immobilized antibody on the conical PET membrane. Besides, a variety of biological methods were used to confirm the effective and specific recognition as well as the spatial conformation of CSTB (antigen) and the antibodies. The corresponding image obtained via X-ray photoelectron spectroscopy (XPS) indicated the diversity of the surface elements of the membrane before and after modification and immunoreaction. The XPS data showed that new N1s and S2p peaks (rectangles in Figure 3B) were formed at approximately 400 and 200 eV, compared to those formed using the unmodified PET membrane (orange

line). N and S are two essential components of amino acids, with N present in all amino acids, and S present in specific amino acids. This also provided a clear evidence of the connection and immunoreaction that occurred on the surface of the planar membrane.^[22] Furthermore, the differences in the curves for the antigens, antibodies, and their mixture could be easily determined using the circular dichroism spectrum (Figure 3C). The result indicated the existence of different secondary structures of proteins in the liquid environment, which could explain the changes in spatial conformation. In addition, we also tested the surface wettability before and after the antigen–antibody reaction. Compared to the blank planar PET film, the functional membrane showed reduced surface wettability and increased water contact angle (WCA) following the antigen–antibody reaction. The WCA on the surface of the functional membrane with only monoclonal antibody modification was $67.5^\circ \pm 1.4^\circ$, whereas it changed to $65.1^\circ \pm 0.4^\circ$ after subsequent connection with CSTB (Figure 3D). Besides, we tested the surface potential of the nano-channel system by Zeta-potential instrument. It was apparent to see that the surface potential was increased with the anchorage of CSTB of different concentration (Figure 3E and Figure S1, Supporting Information). The significant difference in wettability and surface zeta potential indicated the changes in the chemical properties of the membrane system before and after the antigen–antibody binding reaction, which provided a theoretical basis for the precise regulation of the transmembrane current. In summary, the above results suggested that the specific antigen–antibody immunoreaction could be used successfully for the detection of CSTB in saliva specimens.

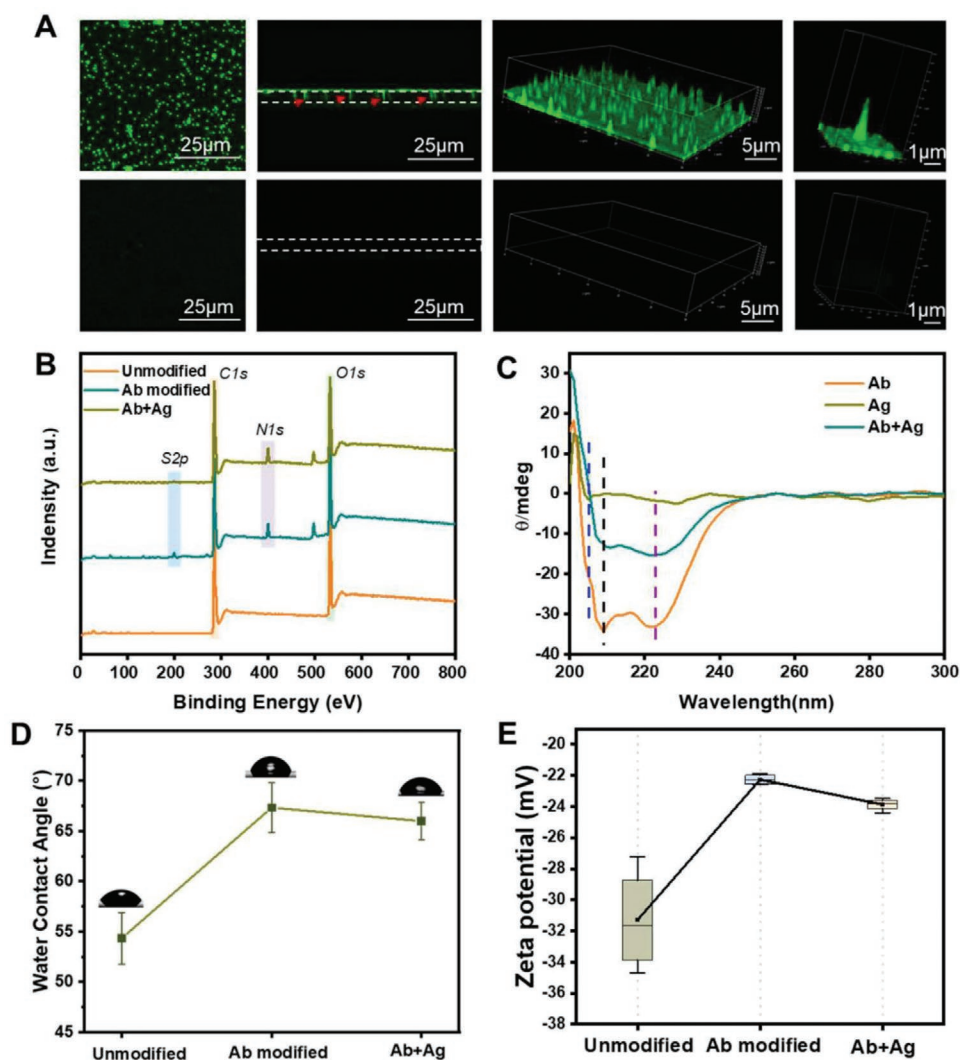


Figure 3. Characterization of CSTB monoclonal antibodies based on immobilization and immunoreaction. A) Observation using laser confocal microscopy confirmed the existence and location of antibodies (top) on the PET membrane after modification, whereas no fluorescence signal was detected without antibody modification (bottom); B) Detection of N and S after antigen–antibody binding using XPS; C) The CD spectrum curve indicated the conformational difference among antibodies, antigens, and their immunoreaction complex. D) Measurement of WCA on PET for antibody-modified, and antibody-antigen binding on flat membrane; E) Measurement of the surface zeta potential on PET membrane with different conditions. Zeta potential was enhanced after the combination of antigen and antibody. CD, circular dichroism; PET, polyethylene terephthalate; WCA, water contact angle; XPS, X-ray photoelectron spectroscopy.

2.3. Conventional Methods for CSTB Detection

Before the nano-channel system was applied for CSTB detection, we initially used conventional testing methods to detect CSTB at different concentrations in the sample preparation. Based on the results obtained using a commercial ELISA kit corresponding to the same CSTB monoclonal antibody, the detection range was approximately 10^{-9} – 10^{-7} g mL⁻¹ (Figure 4A), and the lowest concentration detected using ELISA was 6×10^{-9} g mL⁻¹ (Figure 4B,C). Using the dot blot technique, the tested protein was dot-added to a polyvinylidene fluoride (PVDF) film and made to hybridize with an immobilized protein probe. The protein was hybridized after a series of steps involving membrane washing and autoradiography were performed, and the hybridization intensity was measured. We used

CSTB and its monoclonal antibody as the immobilized protein and probe, respectively, with each element capable of recognizing its counterpart. The results of the dot blot (Figure 4D) showed that both the antibody and the antigen immobilized on the PVDF film could effectively recognize their counterparts in vitro and form corresponding traces based on their concentration by immunoreaction. Of note, the detection range was limited by the end of the experiment (range: $>10^{-8}$ g mL⁻¹).

However, previous studies have demonstrated that the CSTB concentration in saliva was lower than 5×10^{-9} g mL⁻¹ in specimens obtained from healthy individuals and even lower in specimens obtained from patients with metastatic OSCC.^[18,23] Therefore, ELISA and dot blot techniques cannot effectively meet the diagnosis standard required for the accurate detection of CSTB in samples obtained from patients with metastatic

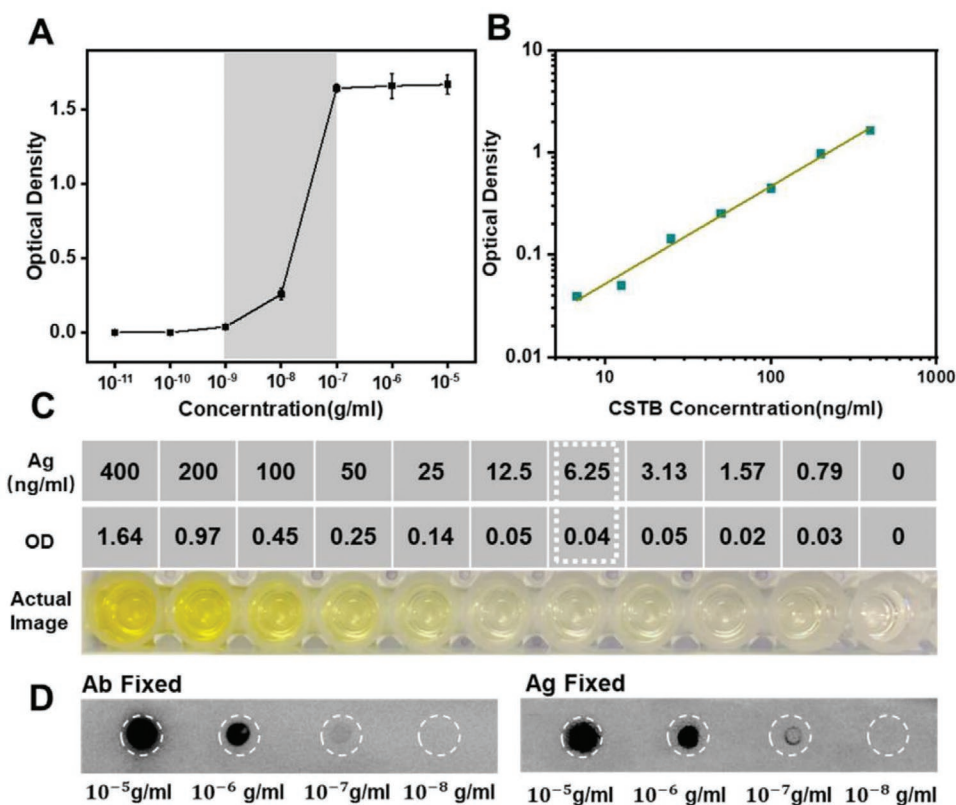


Figure 4. Conventional ELISA or dot blot detection of CSTB is limited by sample concentration (lower than 10^{-8} g mL⁻¹). A–C) ELISA showed a limited testing range of approximately 10^{-9} – 10^{-7} g mL⁻¹ of CSTB. D) Dot blot results showed the specific binding ability of CSTB and anti-CSTB antibody. CSTB at concentrations lower than 10^{-8} g mL⁻¹ could not be detected. CSTB, cystatin B; ELISA, enzyme-linked immunosorbent assay.

OSCC. Besides, the abovementioned detection methods require large quantities of condensed protein and tedious, repetitive procedures, which leads to inefficient detection in real-time monitoring of cancer progression.^[24]

2.4. Detection Performance at Different Concentrations of CSTB and the Underlying Mechanism

Based on the limitations of existing detection methods and the feasibility of using the nano-channel system, we assessed the ability of the functionalized nano-channel to detect CSTB at different concentrations in *in vitro* samples. **Figure 5** shows the detection capability of the system based on *I*–*V* curves of the antibody-functionalized nano-channel membrane after interaction with CSTB in solution. In this study, phosphate buffer solution (PBS), which simulates the physiological buffer environment *in vivo*, was used as an electrolyte and solvent for CSTB for its detection and for construction of standard curves at different concentrations of CSTB. After the asymmetric functionalized nano-channel was manufactured, the spatial structure was observed to be relatively narrow, and the corresponding wettability decreased (Figure 4C). The current curve was smoother (red curve, Figure S2, Supporting Information), and the rectification ratio decreased compared to that in the blank group (black curve, Figure S2, Supporting Information). The ionic currents decreased from -4.2 to -2.6 nA

at -2.0 V or from 1.5 nA to 0.6 nA at 2.0 V (Figure S2, Supporting Information), respectively. Therefore, the nano-channel membrane was immersed in different concentrations of CSTB solution and the transmembrane current was recorded. Based on continuous changes in CSTB concentrations, the detection range of the single-nano-channel system was determined to be 10^{-8} – 10^{-12} g mL⁻¹ (Figure 5A). Within this range, the current curves were distributed successively between the control group (unmodified PET membrane) and the blank group (modified membrane without test) when the antigen concentration decreased gradually from 10^{-8} to 10^{-12} g mL⁻¹, as shown in Figure 5A and Figure S3, Supporting Information. A stable and regular change was observed when the ionic current decreased from -5.5 to -2.6 nA at -2.0 V, as indicated by the statistical data (Figure 5B). In addition to the ionic current curves, the current change ratio ($(I_0 - I)/I_0$) measured at -2.0 V also characterized the antigen–antibody recognition as a response (Figure 5C). With the sequential increase in CSTB concentrations, the ratio of current change increased from 0.13 to 1.06 . A good linear relationship within the range 10^{-9} – 10^{-12} g mL⁻¹ was observed concomitantly ($R^2 = 0.95256$). The above results showed that the designed nano-channel membrane system exhibited high performance in the detection of trace levels of CSTB. In addition, certain interfering non-specific proteins were also analyzed using this nano-channel system to verify the specificity of CSTB detection. The results showed that the current values corresponding to the detection of cystatin C (CST3)

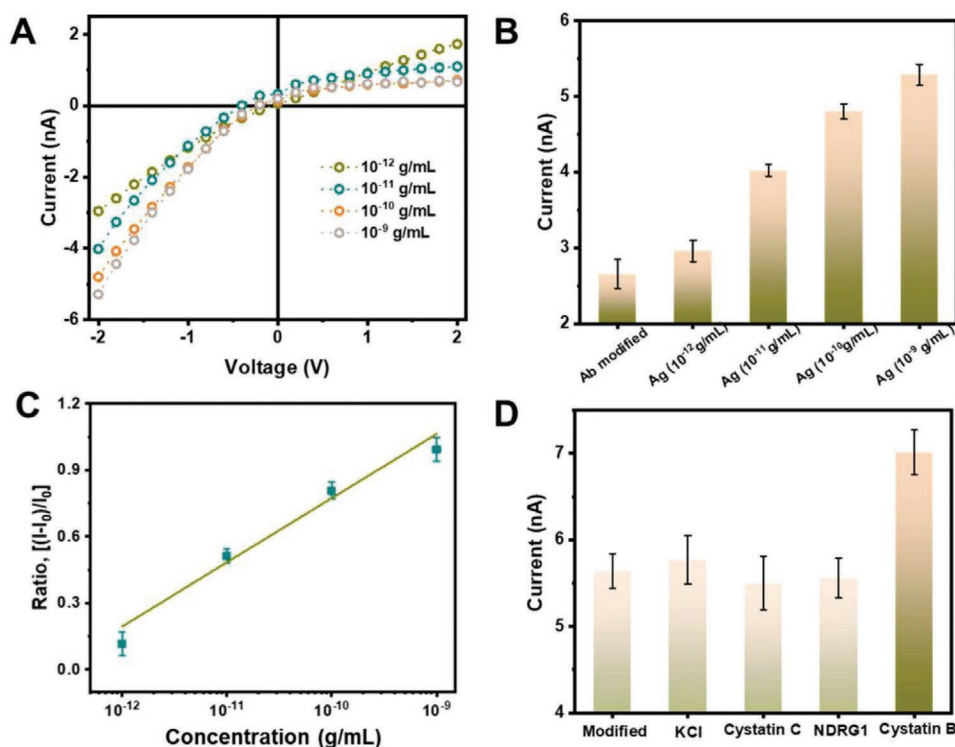


Figure 5. Functionalized asymmetric nano-channels demonstrating improved sensitivity with a detection limit of $10^{-12} \text{ g mL}^{-1}$ and high selectivity for cancer biomarker. A) I - V curves of nano-channels stimulated with CSTB in PBS (10^{-9} – $10^{-12} \text{ g mL}^{-1}$); B) Ionic current variation at -2.0 V through the nano-channels stimulated with CSTB in PBS (10^{-9} – $10^{-12} \text{ g mL}^{-1}$); c) Linear relationship between ionic current ratios ($(I_0 - I)/I_0$) at -2.0 V in functionalized nano-channels at varying CSTB concentrations; D) The nano-channel system showed less specificity for non-specific proteins (CST3 and NDRG1) than for CSTB. CST3, cystatin C; CSTB, cystatin B; NDRG1, *N*-myc downstream-regulated gene 1; PBS, phosphate buffer saline.

and *N*-myc downstream-regulated gene 1 (NDRG1) protein, which are common proteins found in saliva, were lower than those corresponding to CSTB detection (Figure 5D). A specific detection of cancer related biomarker was realized. Meanwhile, the system without antibody modification did not exhibit any changes in current values after immersion into CSTB solution at different concentrations (Figure S4, Supporting Information). It was deduced that the wettability changes and the positive charge accumulation of proteins within the system eventually led to the current variations. Upon recognition of cancer biomarker, the inner wall of nano-channel could undergo a series of changes, which significantly regulated the ion transport through nano-channel, thus showing improved sensitivity with the detection limit of $10^{-12} \text{ g mL}^{-1}$. The subtle changes in CSTB levels in body fluids were successfully monitored. Therefore, the system exhibited the potential for highly specific and sensitive detection of CSTB. The nano-channel system could be considered for prospective application in the quantitative detection of tumor biomarkers in saliva specimens, and would be superior to the other detection methods reported earlier.^[23]

2.5. Assessment of Salivary Samples Obtained from Clinical Patients with OSCC Using the Developed Nano-Channel System

The major significance of this study was the use of the asymmetric nano-channel system for clinical examination in cancer

screening. Saliva samples were collected from healthy individuals, patients with OSCC and patients with metastatic OSCC (Figure 6A, Supporting Information) and were processed without the interference of cells and bacteria (Figure S5, Supporting Information). As shown in Figure 6B, the testing concentrations of CSTB obtained from individuals in the three groups were different, as observed after calculation using the standard curve presented in Figure 5. The average current ratios corresponding to CSTB detection in the three groups were 1.49, 1.00, and 0.37 respectively. A gradient decreasing trend in the three groups indicated the reduction in CSTB concentration in saliva samples obtained from healthy individuals, patients with OSCC, and patients with metastatic OSCC. Based on data from Figure 6B, the representative values of liquid-biopsy diagnosis in the three groups obtained using asymmetric nano-channel system were consistent with the results obtained from the clinical diagnosis of OSCC. The other diagnostic methods (ELISA and dot blot) could not achieve the ultra-sensitivity and effectiveness of the membrane channel system (Figure 6C and Figure S6, Supporting Information).

We believe that the nano-channel system could be used as a potential diagnostic tool with high analytical performance in cancer diagnosis using bio-fluid specimens. The sensitive and effective detection of the biomarker CSTB may assist clinical decision-making in cases of OSCC and its metastasis, which would help improve the prognosis and survival rate of oral cancers.

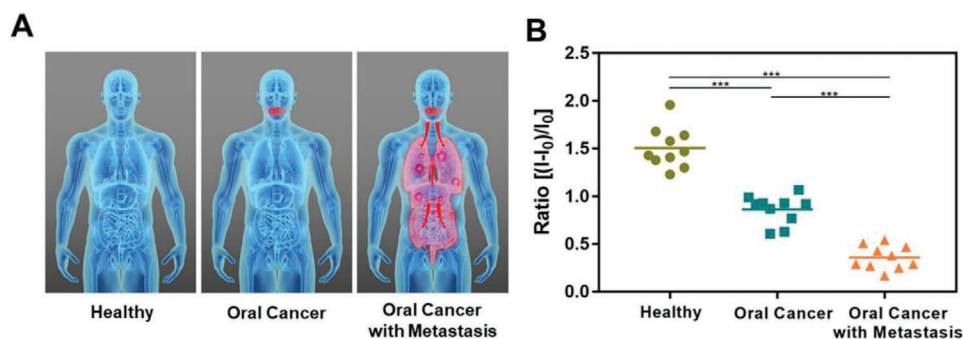


Figure 6. Biopsy of saliva samples collected from clinical patients indicating the sensitivity and selectivity of the functionalized asymmetric nano-channel for the detection of oral cancer and its metastasis. A) Saliva samples obtained from healthy individuals, patients with OSCC, and patients with metastatic OSCC were collected and categorized into three groups. B) A gradually declining trend was presented and could indicate the diagnosis for healthy individuals, patients with OSCC, and patients with metastatic OSCC. Significant differences were observed among the three groups using the nano-channel system (** $p < 0.001$).

3. Conclusion

In summary, a sensitive and effective strategy for cancer biomarker recognition and detection of trace levels of CSTB was successfully designed using the functionalized nano-channel membrane. The process was characterized by the specific immunoreaction and the resultant changes in the trans-membrane ionic current, which indicated high specificity towards CSTB and ultra-sensitivity of the detection limit. Based on the effective performance of the nano-channel membrane system, it could be used to detect the reduction in CSTB levels in saliva samples obtained from patients with oral cancer. The significance of this study is that as a diagnostic tool, the nano-channel system can pave the way for oral cancer metastasis detection in bio-fluid samples. Even though the nano-channel system is now considered as high cost and its detailed material preparation could not reach the satisfaction of in mass production to match the commercial demand. We believe that this effective and specific biomarker detection system could assist clinical decision-making and early detection as a method breakthrough. On this basis, the system with high analytical performance in detecting biomarkers within accessible bio-fluid could be a promising detective choice for real-time monitoring of cancer evolution and therapeutic responses.

4. Experimental Section

Materials: Polymer foils of PET (Hostaphan RN 12, Hoechst) of 12 μm thickness were irradiated at the linear accelerator UNILAC (GSI, Darmstadt) with swift heavy ions (Au) having an energy of 11.4 MeV per nucleon. HCHO and EDA were purchased from Sigma-Aldrich Co. (St. Louis, MO). All solutions were prepared in Milli-Q water (18.2 M Ω).

Fabrication of Conical Nano-Channels: The single channel membrane was mounted in a conductivity device for the asymmetric etching after exposed to the UV light (365 nm, 20 W) for 1 h on each side at room temperature. One side of the facility was filled with 9 M NaOH as etching solution, while the other side was filled with stopping solution made of 1 M KCl and 1 M formic acid, which could neutralize the etchant as soon as the pore opened. During the etching process, the temperature was kept at 30 $^{\circ}\text{C}$. The transmembrane ionic current was used to monitor the etching process. After being etched, the PET membrane was soaked in Milli-Q water to remove residual salts.

Specific-Antibody Functionalized Process: The monoclonal antibody of CSTB (Abcam, USA) was immobilized onto the inner surface of the nano-channels by a two-step chemical reaction. First, the carboxyl groups were activated by immersing the PET membrane in an aqueous solution of EDC (15 mg mL⁻¹) and NHSS (3 mg mL⁻¹) for 1 h at room temperature. Then the membrane was washed with distilled water and immersed into the aqueous solution of 1 \times 10⁻⁶ g mL⁻¹ antibody for 2 h to immobilize the surface. Finally, the CSTB antibody-functionalized single-nano-channel membrane was obtained after washing with phosphate B buffer solution (PBS, Servicebio, China) water and drying by N₂.

Current Measurement: The recognition performances of the nano-channels were studied by monitoring ionic current under the conditions of absence and presence of target molecule. The ionic current was measured by a Keithley 6487 picoammeter (Keithley Instruments, Cleveland, OH). A conical PET membrane was mounted between two halves of the device. Both halves of the cell were filled with aqueous solution of PBS solution. Ag/AgCl electrodes were used to apply a transmembrane potential across the film and the scanning voltage varied from -2 to +2 V. Before each *I*-*V* measurement, the membrane was immersed into the as-prepared solutions for 1 h, followed by washing with deionized water. All the measurements in this work were carried out in the same conditions, and each test was repeated 3 successive times to obtain the average current value. For the concentration testing part, the CSTB protein of different concentration and the saliva samples were dropped onto the membrane. After reaction, the current value was tested on the device.

Sample Characterization: Scanning electron microscopy (SEM) images were captured in the field-emission mode using a Hitachi S-4800 microscope (Japan) at an acceleration voltage of 10 kV. XPS data were recorded with an ESCALab220i-XL electron spectrometer from VG Scientific using 300 W Al K α radiation. All peaks were referenced to C1s (CHx) at 284.8 eV in the deconvoluted high-resolution C1s spectra. Water contact angle (WCA) was measured by an OCA20 instrument (DataPhysics, Germany) at ambient temperature. The WCA values were taken as the averages of five independent measurements of the same sample. Transmission electron microscope (TEM, JEM-1230, JEOL, Tokyo, Japan) was used to test the shape of CSTB, antibody and their mixture. Fifteen milliliters of solution were dropped onto a 400-mesh copper TEM grid covered by a carbon support. Excess liquid was removed by the filter paper beneath the grid. CD spectra was also used for testing of the combination conformation. CD kinetic spectra were collected on a JASCO J-815 CD spectrometer with a bandwidth of 1.0 nm. Immunofluorescence analysis was applied for the morphology of the conical shaped nano-channel and the immobilization of antibodies. Here multi-nano-channel membrane of the same PET material was used for easier detection of channels under laser confocal microscope (Leica, SP8, Germany). The samples were first anchored with antibody as the mentioned step. It was recognized by the secondary antibody labeled with immunofluorescence which was specific to rabbit primary

antibody (Abcam, Ab150081). For surface zeta-potential measurements, membranes with anchored-antibody or further reaction with CSTB were measured using a special surface zeta potential device from Zeta Sizer Nano-ZS Instrument (Malvern Instruments, Worcestershire WR, UK) in an aqueous environment at room temperature. The membrane sample was cut into a rectangle with length of 4 mm and width of 3 mm and glued onto the special bracket. The surface zeta potential measurement was performed according to the manufacturer instructions.

Human Saliva Collection: Healthy people without OSCC, patients with diagnosis of OSCC and OSCC with metastasis (diagnosis confirmed by post-surgery histopathology) were planned to collect the saliva. (ethics approval from IRB of Peking University Hospital of Stomatological: PKUSSIRB-201952182) were centrifuged at 1500 rcf and 4 °C for 5 min, and the supernatant from each sample was further centrifuged at 10 000 rcf and 4 °C for 5 min.^[16] The supernatant was then added dropwise onto the membrane system, and the current value was subsequently tested. All of the donors signed and agreed with informed consent. First morning urine samples of participants were taken before breakfast. Ten milliliters of sample were collected from each participant and immediately placed in a 4 °C refrigerator.

Elisa and Dot Blot Tests: Samples were tested using Elisa and dot blots to verify their concentration as control. Elisa kit of CSTB was synthesized commercially using the consistent CSTB monoclonal antibodies of the whole work. 100 µL of standard or saliva specimen was added to the precoated plate and incubated at 37 °C for 1 h. Following five consecutive wash steps with PBS, 100 mL of horseradish peroxidase labeled avidin was added after five times of washing with PBS and incubated at 37 °C for 30 min. Finally, 50 µL of chromogenic reagent A and B was added in turn after five times of washing with PBS, and then incubated at 37 °C for 15 min. The reaction was stopped by adding 50 µL of sulfuric acid as stop buffer. The OD value of each sample was measured at 450 nm with an LP400 plate meter. The dot-blot immunoassays were performed on a hydrophobic polyvinylidene fluoride (PVDF) membrane (Millipore Immobilon-P, USA). Dilution of CSTB antibody or CSTB protein solution in PBS buffer was spotted on the membrane by placing a pipette tip for the immobilization step of the antigen or antibody. After drying at room temperature for 1 h, the membrane was blocked by incubation in a solution of 5% nonfat dry milk in TBST buffer for 2 h. Then the membranes were incubated with HRP conjugated secondary antibodies (Cell Signal Technology, USA). Autoradiograms were obtained using an ECL dot blot substrate.

Flow Cytometry: Milli-Q water, saliva after centrifugation and saliva was used for flow cytometry (Becton, Dickinson and Company, USA). The machine was cleaned 3 times before every test and 40 µL sample was applied to the selection tube. The events were calculated after the automatic model selection.

Bacterial Colony Count: Milli-Q water, saliva after centrifugation and saliva was used for bacterial colony count. The spiral automatic counting was cleaned three times before every test. 50 µL sample was applied for every test on BHI (Brain Heart Infusion) agar plate and the plates were cultured at 37 °C under 5% CO₂ atmosphere for 48 h.

Statistical Analysis: Comparisons were carried out with paired Student's *t*-tests when two cases were compared, and one-way ANOVA was conducted when more than two conditions were compared. Statistically significant differences were designated as *p*-values <0.05. Statistically significant differences were indicated by * (*p* < 0.05) and *** (*p* < 0.001).

Supporting Information

Supporting Information is available from the Wiley Online Library or from the author.

Acknowledgements

Z.X., C.H. and S.J. contributed equally to this work. This work was supported by the National Key R&D Program of China (2020YFA070049,

2018YFC1105301, 2018YFC1105302, 2018YFC1105304), the National Natural Science Foundation of China (81922019, 51772006, 31670993, 51973004, 81991505, 11874415), the National Youth Topnotch Talent Support Program (QNB)2019-3), Beijing Municipal Science & Technology Commission Projects (Z181100002018001), and the Peking University Medicine Fund (PKU2020LCXQ009). The membranes employed in this work are based on an UMAT experiment, performed at the beam line X0 at the GSI Helmholtzzentrum für Schwerionenforschung, Darmstadt (Germany) in the frame of FAIR Phase 0.

Conflict of Interest

The authors declare no conflict of interest.

Data Availability Statement

Research data are not shared.

Keywords

bio-fluid biopsy, cancer detection, electrochemical, nano-channel

Received: December 3, 2020

Revised: December 29, 2020

Published online:

- [1] B. Freddie, F. Jacques, S. Isabelle, L. Rebecca, A. Lindsey, J. Ahmedin, *CA Cancer J. Clin.* **2018**, *68*, 394.
- [2] G. Carioli, M. Malvezzi, P. Bertuccio, D. Hashim, S. Waxman, E. Negri, P. Boffetta, C. La Vecchia, *Ann. Oncol.* **2019**, *30*, 1344.
- [3] M. M. Siddiqui, S. Rais-Bahrami, B. Turkbey, A. K. George, J. Rothwax, N. Shakir, C. Okoro, D. Raskolnikov, H. L. Parnes, W. M. Linehan, M. J. Merino, R. M. Simo, P. L. Choyke, B. J. Wood, P. A. Pinto, *JAMA, J. Am. Med. Assoc.* **2015**, *313*, 390.
- [4] E. D'Andrea, N. K. Choudhry, B. Raby, G. L. Weinhouse, M. Najafzadeh, *Int. J. Cancer* **2020**, *146*, 781.
- [5] R. Noorlag, K. Boeve, M. J. Witjes, R. Koole R, T. L. Peeters, E. Schuurings, S. M. Willems, R. J. J. van Es, *Head Neck* **2017**, *39*, 326.
- [6] a) A. Salimi, B. Kavosi, F. Fathi, R. Hallaj, *Biosens. Bioelectron.* **2013**, *42*, 439; b) X. P. Zhao, Y. Zhou, Q. W. Zhang, D. R. Yang, C. Wang, X. H. Xia, *Anal. Chem.* **2019**, *91*, 1185.
- [7] a) L. Jing, C. Yang, P. Zhang, J. Zeng, Z. Li, M. Gao, *View* **2020**, *1*, e19; b) J. Yang, Y. Yang, *View* **2020**, *1*, e20.
- [8] J. Marrugo-Ramirez, M. Mir, J. Samitier, *Int. J. Mol. Sci.* **2018**, *19*, 2877.
- [9] a) C. Pei, C. Liu, Y. Wang, D. Cheng, R. Li, W. Shu, C. Zhang, W. Hu, A. Jin, Y. Yang, J. Wan, *Angew. Chem.* **2020**, *59*, 10831; b) L. Huang, L. Wang, X. Hu, S. Chen, Y. Tao, H. S. u, J. Yang, W. Xu, V. Vedarethinam, S. Wu, B. Liu, X. Wan, J. Lou, Q. Wang, K. Qian, *Nat. Commun.* **2020**, *11*, 3556.
- [10] X. Cui, N. Vasylieva, D. Shen, B. Barnych, J. Yang, Q. He, Z. Jiang, S. Zhao, B. D. Hammock, *Analyst* **2018**, *143*, 2057.
- [11] C. Petrovas, S. M. Daskas, E. S. Lianidou, *Clin. Biochem.* **1999**, *32*, 241.
- [12] Z. Ma, S. Skeaff, *Thyroid* **2014**, *24*, 1195.
- [13] A. H. Khan, E. Sadroddiny, *Mol. Cell. Probes* **2016**, *30*, 106.
- [14] Y. T. Cho, H. Su, Y. Y. Chiang, J. Shiea, S. F. Yuan, W. C. Hung, Y. T. Yeh, M. F. Hou, *Clin. Breast Cancer* **2017**, *17*, 373.
- [15] J. Nizioł, J. Sunner, I. Beech, K. Ossoliński, A. Ossolińska, T. Ossoliński, A. Plaza, T. Ruman, *Anal. Chem.* **2020**, *92*, 4251.

- [16] L. Xu, N. Shoaie, F. Jahanpeyma, J. Zhao, K. T. Al-Jamal, *Biosens. Bioelectron.* **2020**, *161*, 112222.
- [17] a) F. Huang, C. Xin, K. Lei, H. Bai, J. Li, Q. Chen, *Cell. Oncol.* **2020**, *43*, 763; b) A. Chi, T. A. Day, B. W. Neville, *Ca-Cancer J. Clin.* **2015**, *65*, 401.
- [18] C. M. Carnielli, C. C. S. Macedo, T. De Rossi, D. C. Granato C. Rivera, R. R. Domingues, B. A. Pauletti, S. Yokoo, H. Heberle, A. F. Busso-Lopes, N. K. Cervigne, I. Sawazaki-Calone, G. V. Meirelles, F. A. Marchi, G. P. Telles, R. Minghim, A. C. P. Ribeiro, T. B. Brandão, G. de Castro, W. A. González-Arriagada, A. Gomes, F. Penteado, A. R. Santos-Silva, M. A. Lopes, P. C. Rodrigues, E. Sundquist, T. Salo, S. D. da Silva, M. A. Alaoui-Jamali, E. Graner, J. W. Fo, R. D. Coletta, A. F. Paes Leme, *Nat. Commun.* **2018**, *9*, 3598.
- [19] a) P. Li, X. Y. Kong, G. Xie, K. Xiao, Z. Zhang, L. Wen, L. Jiang, *Small* **2016**, *12*, 1854; b) X. Lou, Y. Song, R. Liu, Y. Cheng, D. Yong, J. Dai, Q. Chen, P. Gao, Z. Zhao, F. Xia, *Small Methods* **2020**, *4*, 201900432.
- [20] T. Ma, J. Janot, S. Balme, *Small Methods* **2020**, *4*, 2000366.
- [21] a) K. Xiao, G. Xie, P. Li, Q. Liu, G. Hou, Z. Zhang, J. Ma, Y. Tian, L. Wen, L. Jiang, *Adv. Mater.* **2014**, *26*, 6560; b) R. Ren, X. Wang, S. Cai, Y. Zhang, J. B. Edel, *Small Methods* **2020**, *4*, 202000356.
- [22] a) K. Xiao, K. W. Chen, X. Kong, L. Jiang, *Angew. Chem.* **2017**, *130*, 201708695; b) K. Wu, X. Kong, K. Xiao, Y. Wei, C. Zhu, R. Zhou, M. Si, J. Wang, Y. Zhang, L. Wen, *Adv. Funct. Mater.* **2019**, *29*, 1807953.
- [23] H. Xiao, Y. Zhang, Y. Kim, S. Kim, J. J. Kim, K. M. Kim, J. Yoshizawa, L. Y. Fan, C. X. Cao, D. T. Wong, *Sci. Rep.* **2016**, *6*, 22165.
- [24] L. M. T. Phan, R. Rafique, S. H. Baek, T. P. Nguyen, K. Y. Park, E. B. Kim, J. G. Kim, J. P. Park, S. K. Kailasa, H. J. Kim, C. Chung, T. S. Shim, T. J. Park, *Biosens. Bioelectron.* **2018**, *121*, 111.